

AN ENERGY-BASED AXIAL ISOTHERMAL-MECHANICAL FATIGUE LIFING PROCEDURE

John Wertz & M.-H. Herman Shen
Department of Mechanical & Aerospace Engineering
The Ohio State University
Columbus, OH 43210

Onome Scott-Emuakpor, Tommy George,
& Charles Cross
Air Force Research Laboratory
Wright-Patterson AFB, OH 45433

ABSTRACT

An energy-based fatigue lifing procedure for the determination of fatigue life and critical life of in-service structures subjected to axial isothermal-mechanical fatigue (IMF) has been developed. The foundation of this procedure is the energy-based axial room-temperature fatigue model, which states: the total strain energy density accumulated during both a monotonic fracture event and a fatigue process is the same material property. The energy-based axial IMF lifing framework is composed of the following entities: (1) the development of an axial IMF testing capability; (2) the creation of a testing procedure capable of assessing the strain energy accrued during both a monotonic fracture process and a fatigue process at various elevated temperatures; and (3), the incorporation of the effect of temperature into the axial fatigue lifing model. Both an axial IMF capability and a detailed testing procedure were created. The axial IMF capability was employed in conjunction with the monotonic fracture curve testing procedure to produce eight fracture curves at three operating temperatures. The strain energy densities for these fracture curves were compared, leading to the assumption of constant monotonic fracture energy at operating temperatures below the creep activation temperature.

NOMENCLATURE

C	= cyclic curve-fit constant
E	= Young's modulus
N	= cycles to failure
T	= temperature
T_o	= room-temperature
W_c	= cyclic strain energy density
W_m	= monotonic fracture strain energy density
α	= coefficient of thermal expansion
ε_c	= strain, fatigue process
ε_f	= strain at failure
ε_m	= strain, monotonic fracture process
ε_n	= strain at necking

ε_o	= monotonic curve-fit constant
$\varepsilon_{thermal}$	= thermal strain
σ	= stress
σ_a	= stress amplitude
σ_c	= cyclic curve-fit constant
σ_n	= stress at necking
σ_o	= monotonic curve-fit constant
σ_{pp}	= $2 \sigma_a$
σ_u	= applied stress at failure
σ_y	= 0.2% offset stress

INTRODUCTION

Various fatigue lifing schemes have historically been used for the design of aerospace structural components, including stress-versus-cycle (S/N) plots, Goodman diagrams, and modified Goodman diagrams [1]. Derived from large quantities of experimental data, these methods provide reliable lifetime estimates but have the disadvantage of high developmental costs.

A novel approach to the development of a less expensive, more stringent fatigue life prediction method originated in 1923 with the suggestion of applying an energy-based method to fatigue life prediction [2]. This method examines the phenomenon of strain hardening, the plastic or irreversible straining of metal that is characterized by an increase in the stress necessary to produce a defined amount of plastic strain [3]. Due to strain hardening, a portion of the work done on a structure during a fatigue process accumulates as strain energy within the structure. Evidence of this can be found in the existence of a finite area between the loading and unloading stress-strain curves of a specimen oscillated between two stress levels [4].

Attempts to apply this theory remained largely unsuccessful until the development of Stowell's fatigue lifing model in 1966. Stowell's work - founded on principles advanced by Feltner, Morrow and Enomoto - directly accounted for the strain energy accumulation of a fatigued structure through application of strain energy density integrals [4,5]. This model was based on two fundamental assumptions; first, that the damaging energy per cycle for a given stress amplitude is constant and equal to the area under the static

• Corresponding author. Tel.: +1-614-292-2280
E-mail address: shen.1@osu.edu (M.-H. Herman Shen)

stress-plastic strain curve; and second, that the total damaging energy required to cause fatigue fracture is constant and as a first approximation equal to the area under the static-true stress-true strain curve [6].

Stowell's work was expanded by Scott-Emuakpor et al., providing the basis of an improved energy-based fatigue lifing framework for various load paths. Capabilities developed within this framework included axial fatigue life prediction, uniaxial bending fatigue life prediction, and transverse-shear fatigue life prediction [7-9]. As with Stowell, these models made use of strain energy density integrals to compare the accumulated monotonic fracture energy to the energy accumulated during a fatigue process. A framework was developed for both Aluminum (Al) 6061-T6 and Ti-6Al-4V.

Next, Ozaltun et al. and Wertz et al. re-examined the axial and shear models, respectively, to quantify the effects of material softening and/or hardening on the cyclic strain energy accumulation rate [10,11]. Investigations into these two cases led to the development of critical-life prediction models for each case. Figure 1 compares the full-life and critical-life estimations against experimental data for axial fatigue with Al 6061-T6.

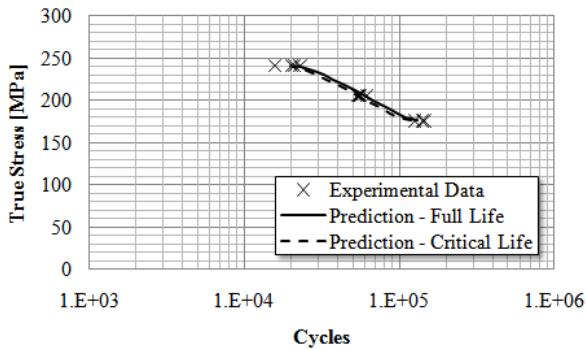


Figure 1. Full-life and critical-life predictions [10].

One distinction of this fatigue lifing framework is the absence of support for elevated temperatures. Each model was developed for room-temperature materials, a practice that reduced modeling complexity at the cost of decreased applicability to real-world problems. Fortunately, the energy-based nature of this framework lends itself to the incorporation of an IMF lifing capability.

Thus, it is through consideration of past work that the objectives of the current study are identified. First, an axial IMF testing capability must be developed. Second, a testing procedure able to assess the strain energy accrued during both monotonic fracture and axial fatigue processes at elevated temperatures must be designed. Third, the effect of elevated temperature must be incorporated into both the full-life and critical-life fatigue lifing models.

FOUNDATIONAL RESEARCH SCOPE

The axial IMF model is a direct evolution of the axial room-temperature fatigue lifing method [7]. This method hinges on the equality between the strain energy density accumulated during both a monotonic fracture process and a fatigue process (Equation 1). Calculation of the two strain energy densities requires two forms of a single constitutive relationship,

presented in Equations 2 & 4, to model the strain induced in a monotonic fracture process (Equations 2 & 3) and a cyclic fatigue process (Equation 4).

$$W_m = NW_c \quad (1)$$

$$\varepsilon_m = \frac{\sigma}{E} + \varepsilon_o \sinh\left(\frac{\sigma}{\sigma_o}\right) \quad (2)$$

$$\sigma_o = \frac{\sigma_n - \sigma_y}{\ln(\varepsilon_n/0.002)} \quad (3)$$

$$\varepsilon_c = \frac{\sigma_{pp}}{E} + \frac{1}{C} \sinh\left(\frac{\sigma_{pp}}{\sigma_c}\right) \quad (4)$$

The strain energy densities accumulated during both the monotonic fracture process and the fatigue process are presented in Equations 5 & 6, respectively.

$$W_m = \alpha \varepsilon_m - \int_0^\sigma \varepsilon_m d\sigma \quad (5)$$

$$W_c = \alpha \varepsilon_c - 2 \int_0^\sigma \varepsilon_c d\sigma \quad (6)$$

Fatigue life is determined from Equation 1 by dividing W_m by W_c . The resulting axial room-temperature fatigue lifing model can be found in Equation 7.

$$N = C \frac{\sigma_u \left(\varepsilon_f - \frac{\sigma_u}{2E} \right) - \sigma_o \varepsilon_o \left[\cosh\left(\frac{\sigma_u}{\sigma_o}\right) - 1 \right]}{2\sigma_c \left\{ \frac{\sigma_a}{\sigma_c} \sinh\left(\frac{2\sigma_a}{\sigma_c}\right) - \left[\cosh\left(\frac{2\sigma_a}{\sigma_c}\right) - 1 \right] \right\}} \quad (7)$$

TEST RIG DESIGN

Design Requirements

The development of an IMF capability requires the synthesis of supporting devices and load frame modifications. The load frame must be altered to physically handle the thermal demands of the testing procedure, requiring the use of specialized grip fixtures. Specimens fitting these specialized grips and conducive to rapid, even heating must be developed. Thermal output must be generated through the use of a heat source, which itself requires an array of supporting devices. Finally, measurement systems must be shielded from both the thermal loading and interference generated by the heat source. Each of these challenges was addressed in the development of the current IMF capability. The load frame is found in Figure 2.

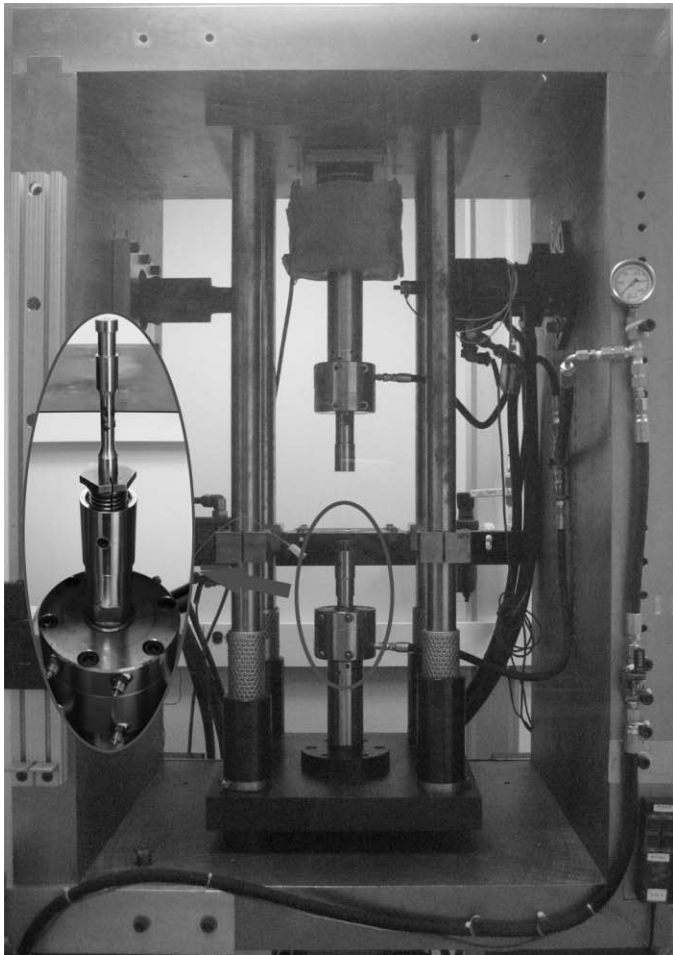


Figure 2. IMF load frame.

Load Frame Alteration

Many load frames utilize hydraulic grips, which feature two advantages; first, the specimen loading and unloading process is simple and efficient; and second, many hydraulic grips are designed to support a wide range of specimen grip-section geometries. However, these grips tend to conduct the thermal load acting on the specimen to internal temperature-sensitive components, imposing limits on the operating temperatures. As an example, MTS 647.10A hydraulic grips have a maximum operating temperature of 65°C.

One solution to this problem is to utilize a set of buttonhead grips (Figure 2, inset). These grips, part of the MTS 652.01 furnace set, are constructed of high temperature alloys aimed at isolating the actuator rod and other sensitive components from the thermal load acting on the specimen. Additionally, these grips feature the option of active cooling, permitting operating temperatures up to 1000°C. Hydraulic pressure from a foot pump is used to operate pistons locking the specimen within the grips.

Specimen Design

ASTM E606: Standard Practice for Strain-Controlled Fatigue Testing provided guidelines for the design of the buttonhead test specimen presented in Figure 3^[12]. Each specimen was computer numerically-controlled (CNC) lathed from a single heat of Al 6061-T6 tube stock. Further surface

treatment was not used due to its negligible effect on fatigue life as studied by Laz et al. and Scott-Emuakpor et al.^[13,14].

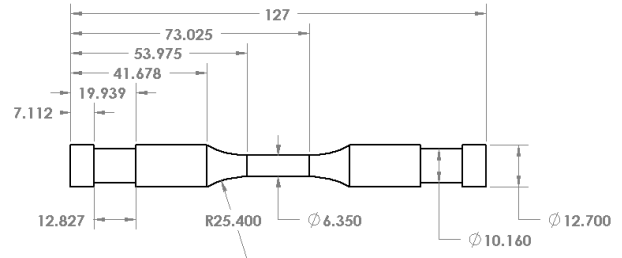


Figure 3. IMF specimen design, dimensions in mm.

Thermal Output and Control

Several options for applying thermal loading were available, including high-temperature furnaces, heat lamps, or induction ovens. Each method boasts both advantages and disadvantages specific to the type of operation it is desired to implement.

For the purpose of this study, the induction heating method was chosen to provide thermal loading. This system is comprised of two components, including an induction oven and a chiller unit to provide cooling. Manufactured by Ambrell, the 5060 6kw induction oven is composed of the power source and the work head. The distinguishing feature of the work head is a hollow copper coil, which carries both the flow of current output by the power source and cooling water discharged by an Electro Impulse RU-399 chiller. The applied current - aided by the coil design - produces a magnetic field that induces heating within the specimen situated within the coil, while the cooling water ensures the work head itself is protected from overheating. The heating rate and operating temperature are proportional to the amount of power applied by the power source. The induction oven system can be found in Figure 4.

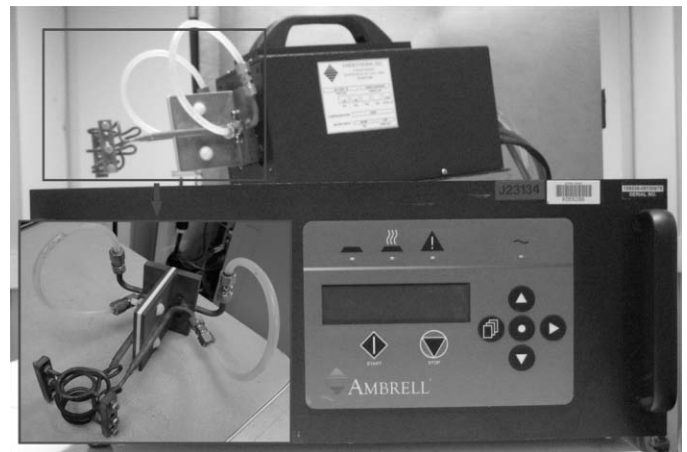


Figure 4. Induction oven system.

The temperature distribution at the surface of the gauge section of a typical specimen was evaluated with three K-type thermocouples cemented below the upper fillet, at the midpoint of the gauge section, and above the lower fillet (Figure 5). Temperature was controlled from TC-2, the thermocouple

located at the center of the gauge section. The results of this study are found in Figure 6.

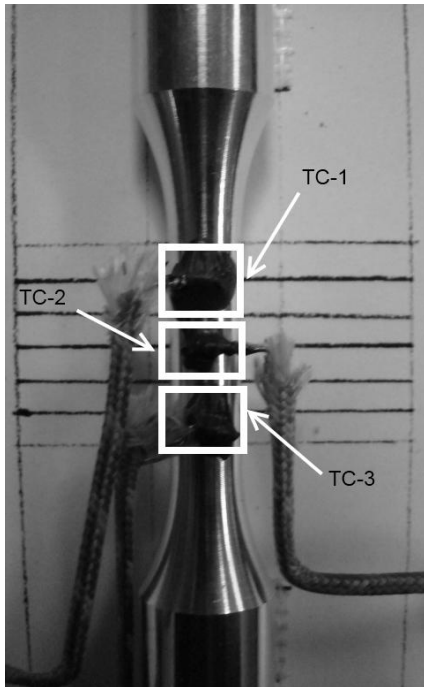


Figure 5. Temperature distribution specimen.

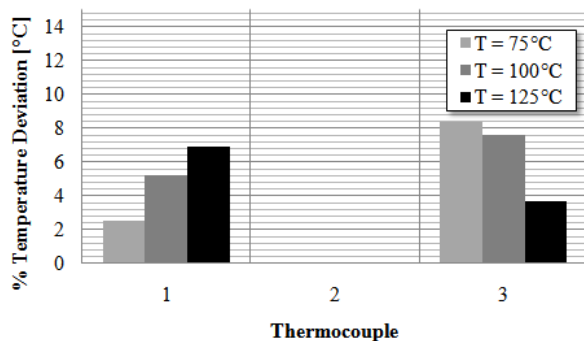


Figure 6. Temperature distribution results.

Data presented in Figure 6 shows an 8.4% maximum surface temperature deviation for a soak period of thirty minutes at 75°C. This deviation is low enough to permit the assumption of constant temperature across the gauge section prior to deformation. Note that the deviation from the demand temperature at TC-2 was zero as the temperature was controlled by that thermocouple.

During testing, temperature control was performed with two K-type thermocouples attached to the surface of the specimen with thermocouple cement. Excessive deformation causes the cement to fail, breaking the bond between the thermocouple and the surface of the specimen. To avoid this problem, the controlling thermocouple was located just above the lower fillet of each specimen. A secondary, non-controlling thermocouple positioned at the midpoint of the gauge section was used to monitor the temperature where deformation was

greatest until the failure of the cement. A typical specimen with this thermocouple arrangement can be found in Figure 7.

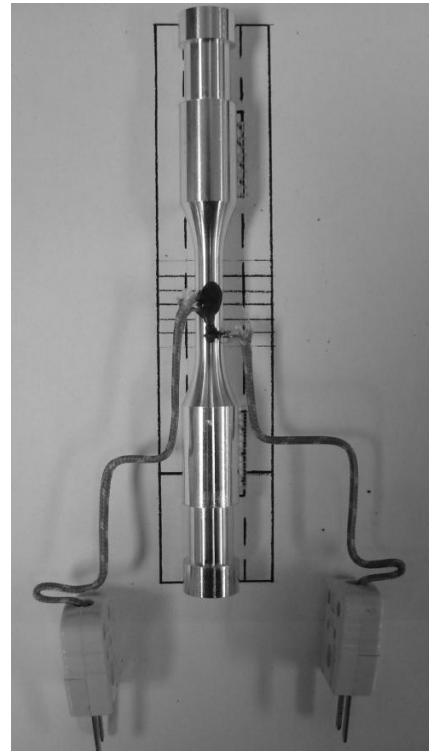


Figure 7. Thermal control study specimen.

A Chino DP1000C digital program controller was used to modulate the applied power of the induction heater based on feedback from the primary thermocouple. The digital temperature controller can be found in Figure 8.



Figure 8. Temperature controller.

Measurement Systems

The combination of both high-temperatures and the magnetic field generated by the induction oven created an environment hostile to measurement systems. Thus, special devices and/or shielding methods were employed to avoid damage or interference.

Three measurement devices were used for this study. Load data was collected with an MTS 661 load cell. This data was conditioned using a Vishay 2360 signal conditioner and passed to an Instron Labtronic 8800 controller. Aggressive grounding practices were observed to isolate the load cell from

interference; additionally, a Faraday cage was constructed to protect the load cell from interference produced by the magnetic field, without which significant spikes in load were observed during operation of the oven with no specimen present. Experimental strain was recorded with an Epsilon 3648 high-temperature capacitive extensometer, which employs long ceramic rods to isolate the body of the extensometer from both the thermal load and interference caused by the magnetic field (Figure 9). Strain data was passed through an Epsilon 3603 signal conditioner before being routed to the Instron controller. Position information was acquired with a Linear Variable Differential Transformer (LVDT) located at the base of the load frame and was passed directly to the Instron controller. Due to its location and the use of buttonhead grips, the LVDT was completely isolated from the operating temperature and magnetic field.

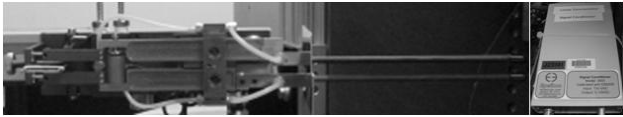


Figure 9. Extensometer system.

Testing Conditions

The load frame was aligned using an MTS 609 alignment fixture in conjunction with a strain-gauged alignment specimen (Figure 10), ensuring the alignment was within the 5% band permitted by *ASTM E466: Standard Practice for Conducting Force Controlled Constant Amplitude Axial Fatigue Tests of Metallic Materials* ^[15].

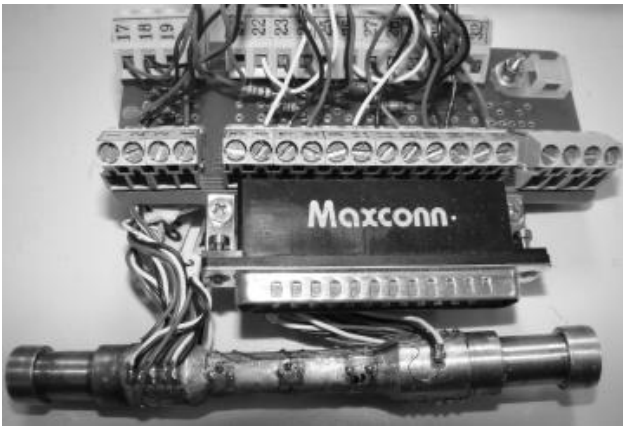


Figure 10. Alignment specimen.

Inconsistencies between tests were minimized through the application of a defined test procedure. This procedure detailed the positioning of the thermocouple on the specimen gauge section, the orientation of the specimen within the buttonhead grips, and the grip pressure used to hold the specimen in place. Proportional-integral-derivative (PID) values of both the Instron and Chino controllers were optimized at the start of the study.

TESTING METHODS

Four testing methods are required to support the development of an IMF lifing capability. These methods include: (1) monotonic fracture tests; (2) basic fatigue tests; (3)

frequency sweeps; and (4), continuous cyclic loading to fatigue failure with constant data acquisition. These tests are designed to be performed at four temperatures, chosen to remain below the creep activation temperature of Al 6061-T6 of 150°C ^[16]. Thus, temperatures of $T_0=25^\circ\text{C}$ (room-temperature), $T_1=75^\circ\text{C}$, $T_2=100^\circ\text{C}$, and $T_3=125^\circ\text{C}$ were used. Isothermal loading was applied to each specimen for thirty minutes prior to initiation of testing. This soak period allows the temperature within the gauge length to equilibrate to the desired operating temperature.

Monotonic Fracture Testing

The strain energy accumulated during a monotonic fracture process is a core component of the energy-based prediction method, forming the numerator of the fatigue lifing equation. Thus, monotonic stress-strain curves must be developed to generate material constants and curve-fit coefficients required by the energy-based method.

Fatigue Testing

Experimental lifetime data provides a basis for validation of the energy-based method at multiple stress levels.

Frequency Sweeps

The heart of the energy-based fatigue lifing theory is the connection between fatigue damage and strain energy accumulation; however, not all of the applied mechanical loading results in actual fatigue damage. In fact, the strain energy derived from an experimental cyclic stress-strain curve (hysteresis loop) is a combination of both plastic and anelastic behavior. Anelastic behavior is due to strain recoverable as a function of temperature and time; thus, strain energy accumulated due to anelastic behavior is non-damaging ^[17]. Being non-damaging, anelastic behavior plays a negligible role in the mechanical damage scrutinized by energy-based theories. For this reason, its effect must be minimized to accurately capture only the cyclic plastic damage ^[4].

The primary method of reducing the presence of anelastic behavior during fatigue is to operate the fatigue process at an ideal frequency. This ideal frequency is identified with a frequency sweep, where a specimen is fatigued across several operating frequencies to generate hysteresis loop data. The operating frequency resulting in the lowest cyclic strain energy is the ideal frequency ^[10,11]. Because anelastic behavior is temperature dependent, it is vital that a frequency sweep be performed at each operating temperature.

Continuous Fatigue Tests (Energy Accumulation History)

By performing continuous fatigue tests at the ideal operating frequency, it is possible to examine the variation in strain energy accumulation rate over the duration of the fatigue process. This variation is attributable to material hardening or softening. Using this information, it is possible to develop a critical life prediction by examining how the energy accumulation accelerates near fatigue failure ^[10,11]. In addition, these tests generate hysteresis loops which are used to determine curve-fit coefficients.

MONOTONIC FRACTURE TEST RESULTS

Monotonic fracture tests were displacement controlled at a rate of 0.001in./second to failure, where failure was defined as the point at which specimens separated completely. Data was accumulated at a rate of 10 samples/second, providing smooth curves for analysis. Monotonic fracture curves at temperatures T_0 , T_1 , and T_2 are presented in Figure 11.

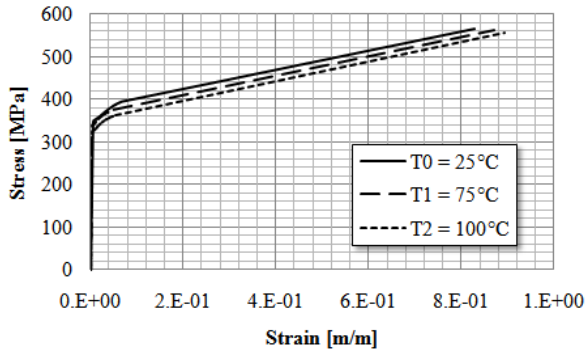


Figure 11. Monotonic fracture curves at temperatures T_0 , T_1 , and T_2 .

Figure 11 suggests that, below the creep activation temperature, the primary effect of temperature on the monotonic fracture curve is to decrease the ultimate stress and increase the ductility. The total strain energy densities of eight monotonic fracture tests - four at T_0 and two each at T_1 and T_2 - are presented in Table 1.

Temperature	Monotonic Fracture Energy
[-]	[MJ/m ³]
T_0	433
	389
	419
	385
T_1	384
	403
T_2	405
	451

Table 1. Total strain energy density at temperatures T_0 , T_1 , and T_2 .

No clear trend is visible in the distribution of strain energy density with operating temperature. Additionally, the averaged strain energy densities developed at temperatures T_1 and T_2 fall within one standard deviation of a normalized distribution generated by data at temperature T_0 as shown in Figure 12. Thus, for operating temperatures below the creep activation temperature, it is assumed that the strain energy density accumulated during a monotonic fracture test is constant. This constancy can be attributed to the way in which, at elevated temperature, increasing ductility offsets decreasing ultimate stress.

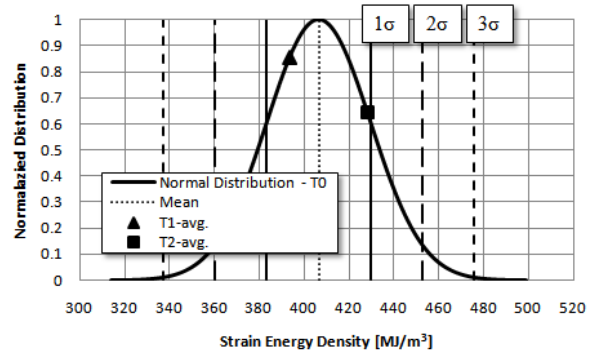


Figure 12. T_1 & T_2 average strain energy density versus T_0 strain energy density normal distribution.

AN ENERGY-BASED AXIAL IMF LIFING CRITERION

Initial Boundary Conditions

Prior to thermal loading, the extensometer is placed in contact with the specimen. As thermal loading begins, the experimental control system is set to load control with a set-point of zero. Thus, as thermal strain accumulates within the specimen, the zero load set-point does not permit the development of thermal stress. Thus, during initial thermal loading, the specimen can be said to experience a "free-free"-type boundary condition. The effect of this boundary condition on both the monotonic fracture curve and the fatigue hysteresis loop can be found in Figures 13 & 14, respectively.

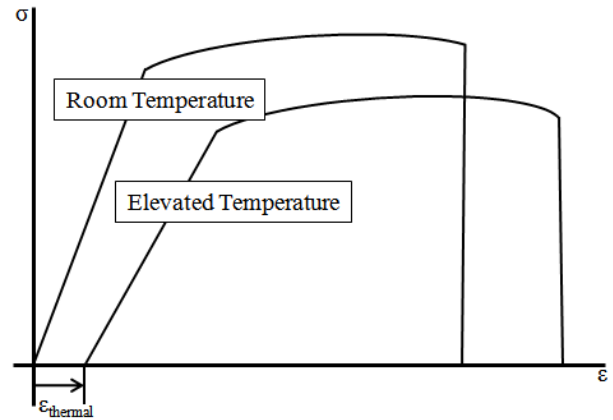


Figure 13. Effect of free-free boundary condition on engineering monotonic fracture curve.

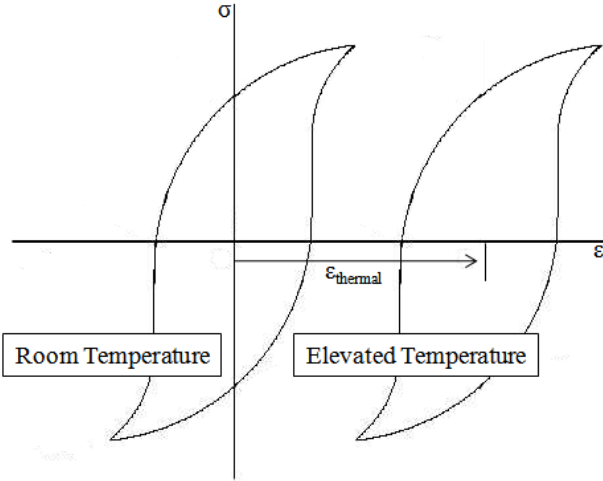


Figure 14. Effect of free-free boundary condition on fatigue hysteresis loop.

From Figure 13, it is clear that the effect of the free-free boundary condition on the monotonic fracture curve is to push the origin of the curve to an initial non-zero strain value. It should be noted that although an initial thermal strain is present, it does not contribute to the total energy to fracture. This is because the free-free boundary causes the initial thermal strain to occur without thermal stress.

From Figure 14, it can be seen that the effect of the free-free boundary condition on the fatigue hysteresis loop is to center the hysteresis loop on a non-zero strain value. Ostensibly, the thermal strain acts as a mean strain; however, again the thermal strain does not contribute to the total hysteresis loop energy.

Considering these two insights, it can be seen that the initial free-free boundary condition removes any contribution by the thermal strain to either the monotonic fracture or fatigue strain energy.

Development of an Axial IMF Lifting Model

To predict IMF life, the effect of temperature must be incorporated into the existing axial room-temperature lifing model. As such, two significant changes must be applied to the room-temperature theory; first, each constant - material or curve-fit - must be allowed to vary with temperature; and second, for the initial free-free boundary condition, the contribution of thermal strain must be removed from the total strain.

The basic governing Equations (Equations 1-4) are restated in Equations 8-11 as a function of temperature.

$$W_m(T) = N(T)W_c(T) \quad (8)$$

$$\varepsilon_m = \frac{\sigma}{E(T)} + \varepsilon_o(T) \sinh\left(\frac{\sigma}{\sigma_o(T)}\right) \quad (9)$$

$$\sigma_o = \frac{\sigma_n(T) - \sigma_y(T)}{\ln(\varepsilon_n(T)/0.002)} \quad (10)$$

$$\varepsilon_c = \frac{\sigma_{pp}}{E(T)} + \frac{1}{C(T)} \sinh\left(\frac{\sigma_{pp}}{\sigma_c(T)}\right) \quad (11)$$

The modification of the monotonic fracture strain energy, W_m , and the fatigue strain energy, W_c , are presented in Equations 12 & 13 and graphically in Figures 15 & 16.

$$W_m(T) = \sigma(\varepsilon_m - \varepsilon_{thermal}) - \int_0^\sigma (\varepsilon_m - \varepsilon_{thermal}) d\sigma \quad (12)$$

$$W_c(T) = \sigma(\varepsilon_c - \varepsilon_{thermal}) - 2 \int_0^\sigma (\varepsilon_c - \varepsilon_{thermal}) d\sigma \quad (13)$$

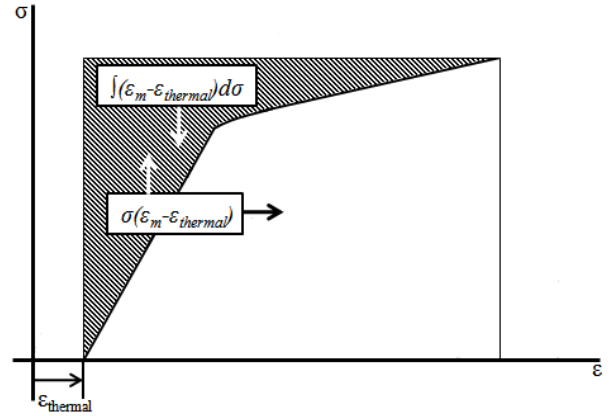


Figure 15. Monotonic fracture strain energy density.

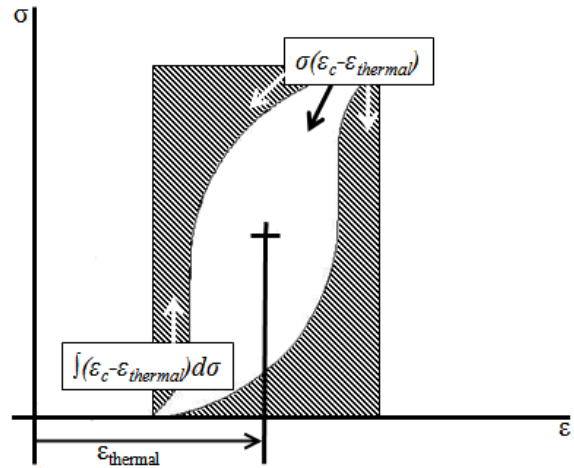


Figure 16. Cyclic strain energy density.

By substituting Equation 14 for $\varepsilon_{thermal}$ and dividing $W_m(T)$ by $W_c(T)$, the axial lifing equation for isothermal-mechanical fatigue is developed (Equation 15).

$$\varepsilon_{thermal} = \alpha(T)(T - T_o) \quad (14)$$

$$N(T) = \frac{\sigma_u(T) \left(\varepsilon_f(T) - \frac{\sigma_u(T)}{2E(T)} \right) - \sigma_o(T) \varepsilon_o(T) \left[\cosh \left(\frac{\sigma_u(T)}{\sigma_o(T)} \right) - 1 \right]}{2 \frac{\sigma_c(T)}{C(T)} \left\{ \frac{\sigma_a}{\sigma_c(T)} \sinh \left(\frac{2\sigma_a}{\sigma_c(T)} \right) - \left[\cosh \left(\frac{2\sigma_a}{\sigma_c(T)} \right) - 1 \right] \right\} + \alpha(T)(T - T_o)} \quad (15)$$

CONCLUSION

Each component of the axial IMF lifing procedure was developed. A testing capability with the capacity to endure the temperatures and interference inherent to an induction-based high-temperature testing environment was established. Additionally, a procedure for determining the parameters of the axial IMF lifing method - as well as the development of that method from the underpinnings of the axial room-temperature fatigue lifing method - was achieved. Monotonic fracture data was analyzed, indicating that it can be assumed that the monotonic fracture energy is constant for temperatures below the creep activation temperature.

With the preliminary work complete, it is now possible to apply this procedure to the remainder of the experimental testing and validate the axial IMF lifing theory. In addition, this foundational work provides a basis upon which thermo-mechanical fatigue (TMF) analyses can be performed.

ACKNOWLEDGEMENTS

The authors would like to thank the Dayton Area Graduate Student Institute (DAGSI) for their financial support of these endeavors. Additionally, the authors would like to thank the Air Force Research Laboratory (AFRL), specifically the Turbine Engine Fatigue Facility (TEFF) laboratory, facility and equipment access, and encouragement of this research. Special thanks to both Phil Johnson and Angela Still, whose support in the development of the IMF capability was critical.

REFERENCES

- [1] Goodman, J. *Mechanics Applied to Engineering*. London: Longmans, Green, and Co., London, 1899.
- [2] Jasper, T. "The Value of the Energy Relation in Testing of Ferrous Metals at Varying Ranges of Stress and at Intermediate High Temperatures." *The London, Edinburgh and Dublin Philosophical Magazine and Journal of Science*. 46. (1923): 609-627.
- [3] Hanstock, R. "Damping Capacity, Strain Hardening and Fatigue." *Proceedings, Physical Society*. 59, Issue 2. (1947): 275-287.
- [4] Feltner, C. and Morrow, J. "Microplastic Strain Hysteresis Energy as a Criterion for Fatigue Fracture." *Journal of Basic Engineering*. (1961): 15-22.
- [5] Enomoto, N. "On Fatigue Tests Under Progressive Stress." *ASTM*. 55. (1955): 903-917.
- [6] Stowell, E. "Energy Criterion for Fatigue." *Nuclear Engineering and Design*. 3, Issue 1. (1966): 32-40.
- [7] Scott-Emuakpor, O., Shen, M.-H. H., Cross, C., Calcaterra, J., and George, T. "Development of An Improved High Cycle Fatigue Criterion." *ASME Journal of Engineering for Gas Turbines and Power*. 129, Issue 1. (2007): 162-169.
- [8] Scott-Emuakpor, O., Shen, M.-H. H., George, T., Cross, C., and Calcaterra, J. "An Energy-Based Uniaxial Fatigue Life Prediction Method for Commonly Used Gas Turbine Engine Materials." *ASME Journal of Engineering for Gas Turbines and Power*. 130, Issue 6. (2008).
- [9] Scott-Emuakpor, O., Shen, M.-H. H., George, T., and Cross, C. "Multi-Axial Fatigue-Life Prediction via a Strain-Energy Method." *AIAA*. 48, Issue 1. (2009): 63-72.
- [10] Ozaltun, H., Shen, M.-H. H., George, T., and Cross, C. "An Energy Based Fatigue Life Prediction Framework for In-Service Structural Components." *Experimental Mechanics*. Published online. (May 25 2010): 1-12.
- [11] Wertz, J. Shen, M.-H. H., George, T., Cross, C., and Scott-Emuakpor, O. "An Energy-Based Experimental-Analytical Torsional Fatigue Life-Prediction Method." *ASME/IGTI*. GT2010-22647. (2010).
- [12] American Society for Test and Materials, (2008), ASTM E606: "Standard Practice for Strain-Controlled Fatigue Testing." *Book of Standards*. 03.01.
- [13] Laz, P. and Hillberry, B. "Fatigue Life Prediction from Inclusion Initiated Cracks." *International Journal of Fatigue*. 20. (1998): 263-270.
- [14] Scott-Emuakpor, O., George, T., and Cross, C. "The Effects on Fatigue Life of Aluminum Based on Surface Conditions." *PHM Society Annual Conference, San Diego, CA*. (2009).
- [15] American Society for Test and Materials, (2007), ASTM E466: "Standard Practice for Conducting Force Controlled Constant Amplitude Fatigue Tests of Metallic Materials." *Book of Standards*. 03.01.
- [16] American Society for Metals, 2002. *Failure Analysis and Prevention: Creep and Stress Rupture Failures*. Vol. 11. American Society for Metals, Metals Park, OH.
- [17] Dieter, G. *Mechanical Metallurgy*. Boston: McGraw-Hill, Boston, 1986.